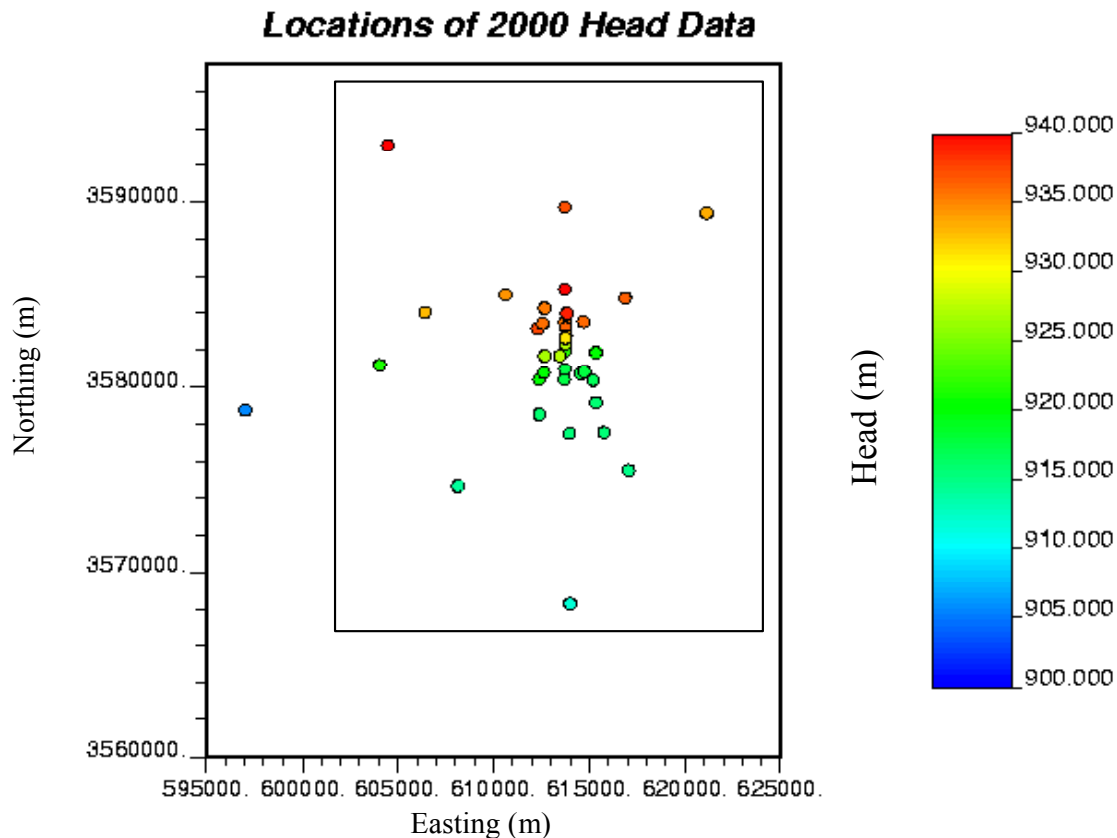


1 **TFIELD-6.2 Initial Heads**

2 A set of initial head values was estimated across the flow model domain based on water-level
 3 measurements made in late 2000 (Beauheim 2002b). The water-level measurements were
 4 converted to freshwater heads using fluid-density data collected from pressure-density surveys
 5 performed in the wells and/or from water-quality sampling. The head values estimated at the
 6 cells in the interior of the domain were used as initial values of the heads and were subsequently
 7 updated by the groundwater flow model until the final solution was achieved. The head values
 8 estimated for the fixed-head cells along the north, east, and south boundaries of the model
 9 domain remained constant for the groundwater flow calculation. The estimation of the initial
 10 and boundary heads was done by kriging. Observed heads both within and outside of the flow
 11 model domain (Figure TFIELD-16) were used in the kriging process.



12

13 **Figure TFIELD-16. Locations and Values of the 2000 Head Measurements Considered in**
 14 **the Steady-State Calibrations. The approximate extent of the numerical model domain is**
 15 **shown by the black rectangle in the image.**

16 Kriging is a geostatistical estimation technique that uses a variogram model to estimate values of
 17 a sampled property at unsampled locations. Kriging is designed for the estimation of stationary
 18 fields (see Goovaerts 1997); however, the available head data show a significant trend (non-
 19 stationary behavior) from high head in the northern part of the domain to low head in the
 20 southern part of the domain. This behavior is typical of groundwater head values measured
 21 across a large area with a head gradient. To use kriging with this type of non-stationary data, a

1 Gaussian polynomial function is fit to the data, and the differences between the polynomial and
 2 the measured data (the “residuals”) are calculated and a variogram of the residuals is constructed.
 3 This variogram and a kriging algorithm are then used to estimate the value of the residual at all
 4 locations within a domain. The final step in the process is to add the trend from the previously
 5 defined polynomial to the estimated residuals to get the final head estimates. This head
 6 estimation process is similar to that used in the Culebra calculations done for the CCA (Lavenue
 7 1996).

8 The available head data from late 2000, comprising 37 measurements, are listed in Table
 9 TFIELD-5. In general, these head measurements show a trend from high head in the north to
 10 low head in the south. The trend was modeled with a bivariate Gaussian function. The use of
 11 this Gaussian function with five estimated parameters allows considerable flexibility in the shape
 12 of the trend that can be fit through the observed data. The value of the Gaussian function, Z , is:

$$13 \quad Z = a \exp \left[-\frac{1}{2} \left(\left(\frac{X - X_0}{b} \right)^2 + \left(\frac{Y - Y_0}{c} \right)^2 \right) \right] \quad (7)$$

14 where X_0 and Y_0 are the coordinates of the center of the function and b and c are the standard
 15 deviations of the function in the X (east-west) and Y (north-south) directions, respectively. The
 16 parameter a controls the height of the function. The Gaussian function was fit to the data using
 17 the regression wizard tool in the SigmaPlot 2001 graphing software. The parameters estimated
 18 for the Gaussian function are presented in Table TFIELD-6. The fit of the Gaussian trend
 19 surface to the 2000 heads is shown in Figure TFIELD-17. The locations and values of the
 20 residuals (observed value – trend surface estimate) are shown in Figure TFIELD-18.

21 The next step in estimating the initial head values is to calculate an experimental variogram for
 22 each set of residuals and then fit a variogram model to each experimental variogram. Due to the
 23 rather limited number of data points, anisotropy in the spatial correlation of the residuals was not
 24 examined and an omnidirectional variogram was calculated. These calculations were done using
 25 the VarioWin[®] (version 2.21) software (Pannatier 1996). The Gaussian variogram model is:

$$26 \quad \gamma(h) = C \left[1 - \exp \left(-\frac{3h^2}{a^2} \right) \right] \text{ for } h > 0 \quad (8)$$

27 where C is the sill of the variogram, h is the distance between any two samples, or the lag
 28 spacing, and a is the practical range of the variogram, or the distance at which the model reaches
 29 95 percent of the value of C . In addition to the sill and range, the variogram model may also
 30 have a non-zero intercept with the gamma (γ) axis of the variogram plot known as the nugget.
 31 Due to numerical instabilities in the kriging process associated with the Gaussian model without
 32 a nugget value, a small nugget was used in fitting each of the variogram models. The model
 33 variogram was fit to the experimental data (Figure TFIELD-19) and the parameters of this model
 34 are given in Table TFIELD-7.

35

1
2**Table TFIELD-5. Well Names and Locations of the 37 Head Measurements Obtained in Late 2000 Used to Define Boundary and Initial Heads**

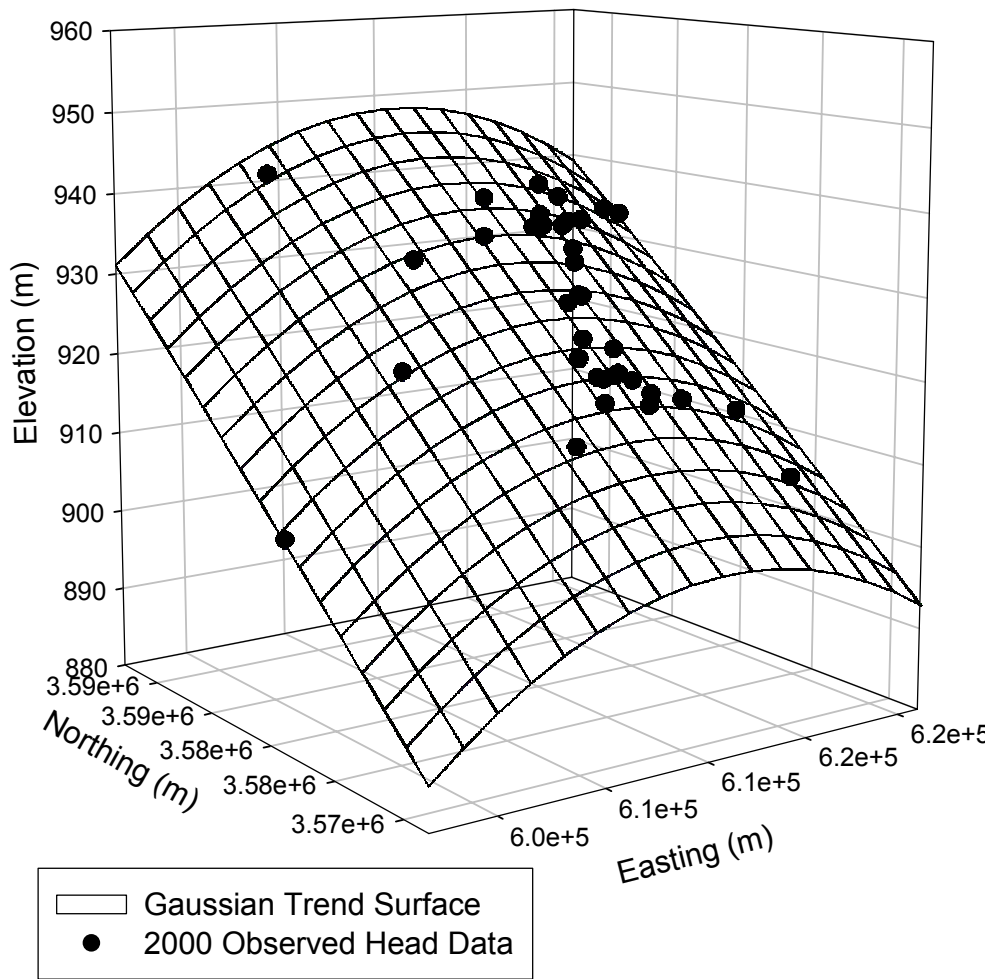
Well	UTM X (Easting) (m)	UTM Y (Northing) (m)	2000 Freshwater Head (m amsl)
AEC-7	621126	3589381	933.19
DOE-1	615203	3580333	916.55
DOE-2	613683	3585294	940.03
ERDA-9	613696	3581958	921.59
H-1	613423	3581684	927.19
H-2b2	612661	3581649	926.62
H-3b2	613701	3580906	917.16
H-4b	612380	3578483	915.55
H-5b	616872	3584801	936.26
H-6b	610594	3585008	934.20
H-7b1	608124	3574648	913.86
H-9b	613989	3568261	911.57
H-11b4	615301	3579131	915.47
H-12	617023	3575452	914.66
H-14	612341	3580354	920.24
H-15	615315	3581859	919.87
H-17	615718	3577513	915.37
H-18	612264	3583166	937.22
H-19b0	614514	3580716	917.13
P-17	613926	3577466	915.20
WIPP-12	613710	3583524	935.30
WIPP-13	612644	3584247	935.17
WIPP-18	613735	3583179	936.08
WIPP-19	613739	3582782	932.66
WIPP-21	613743	3582319	927.00
WIPP-22	613739	3582653	930.96
WIPP-25	606385	3584028	932.70
WIPP-26	604014	3581162	921.06
WIPP-27	604426	3593079	941.01
WIPP-29	596981	3578701	905.36
WIPP-30	613721	3589701	936.88
WQSP-1	612561	3583427	935.64
WQSP-2	613776	3583973	938.82
WQSP-3	614686	3583518	935.89
WQSP-4	614728	3580766	917.49
WQSP-5	613668	3580353	917.22
WQSP-6	612605	3580736	920.02

3

1 **Table TFIELD-6. Parameters for the Gaussian Trend Surface Model Fit to the 2000 Heads**

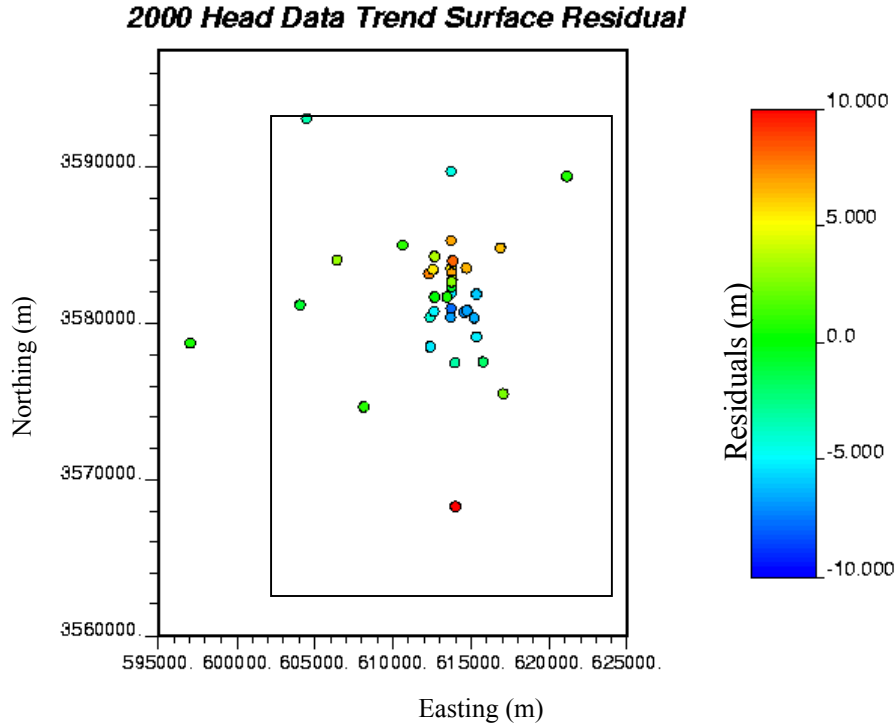
Trend Surface Parameters	Value
X_0	611011.89
Y_0	3780891.50
a	1134.61
b	73559.35
c	313474.40

2



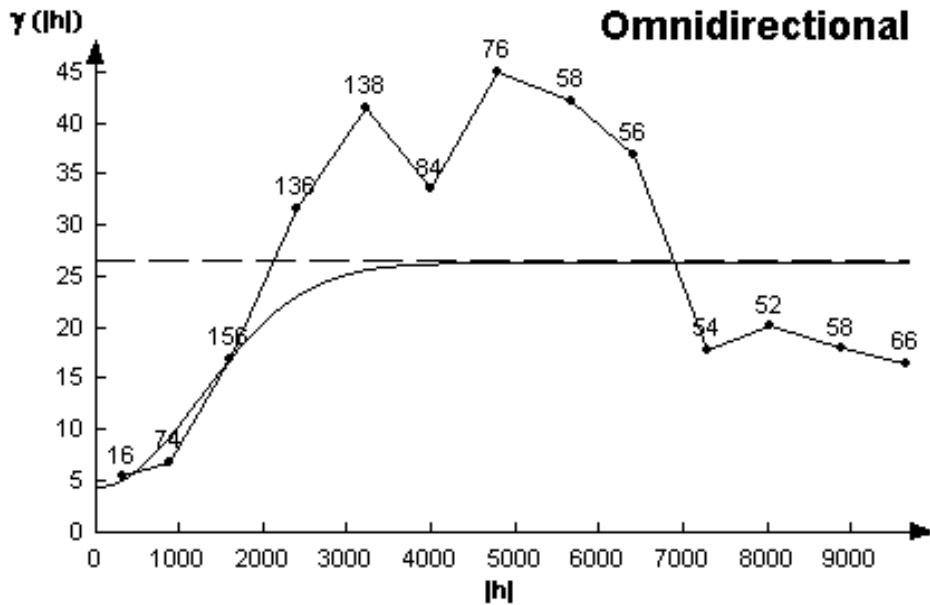
3

4 **Figure TFIELD-17. Gaussian Trend Surface Fit to the 2000 Observed Heads**



1
2
3
4
5

Figure TFIELD-18. Locations and Values of the Residuals Between the Gaussian Trend Surface Model and the Observed Head Data. The approximate boundary of the flow model is shown as a black rectangle in the image.



6
7
8
9
10

Figure TFIELD-19. Omnidirectional Experimental (Straight-Line Segments) and Model Variograms of the Head Residuals (Curves) for the 2000 Heads. The numbers indicate the number of pairs of values that were used to calculate each point and the horizontal dashed line denotes the variance of the residual data set.

Table TFIELD-7. Model Variogram Parameters for the Head Residuals

Parameter	Value
Sill	22
Range (meters)	3000
Nugget	4.5
Number of Data	37

The experimental variogram calculated on the 2000 data in Figure TFIELD-19 shows a number of points between lags 2,000 and 7,000 m (1.25 and 4.25 mi) that are above the variance of the data set (the horizontal dashed line). This behavior indicates that the Gaussian trend surface model used to calculate the residuals from the measured data did not remove the entire trend inherent in the observed data. A higher order trend surface model could be applied to these data to remove more of the trend, but the Gaussian trend surface model provides a reasonable estimate of the trend in the data.

The GSLIB kriging program kt3d (Deutsch and Journel 1998) was used to estimate the residual values at all points on the grid within the model domain. The Gaussian trend surface was then added to the estimated residual values to produce the final estimates of the initial head field.

***TFIELD-6.3* Boundary Conditions**

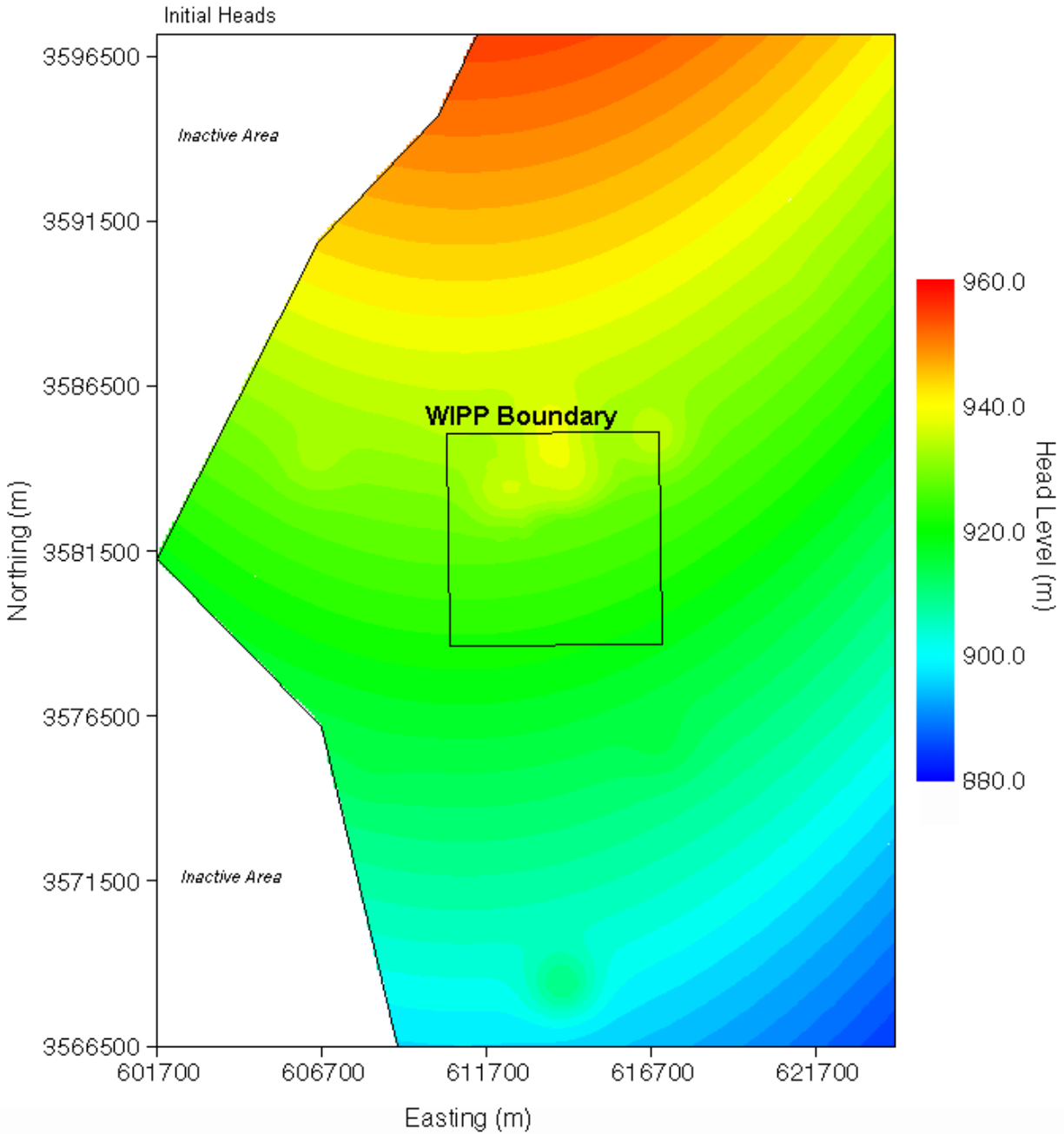
Two types of boundary conditions were specified in MODFLOW-2000: constant-head and no-flow. Constant-head conditions were assigned along the eastern boundary of the model domain, and along the central and eastern portions of the northern and southern boundaries. Values of these heads were obtained from the kriged initial head field. The western model boundary passes through the IMC tailings pond (Laguna Uno) due west of the WIPP site in Nash Draw. A no-flow boundary (a flow line) is specified in the model from this tailings pond up the axis of Nash Draw to the northeast, reflecting the concept that groundwater flows down the axis of Nash Draw, forming a groundwater divide. Similarly, another no-flow boundary is specified from the tailings pond down the axis of the southeastern arm of Nash Draw to the southern model boundary, coinciding with a flow line in the regional modeling of Corbet and Knupp (1996). Thus, the northwestern and southwestern corners of the modeling domain are specified as inactive cells in MODFLOW-2000. The initial (starting) head field is shown in Figure TFIELD-20 and the head values along each boundary of the model domain are shown in Figures TFIELD-21 and TFIELD-22.

***TFIELD-6.4* Observed Steady-State and Transient Head Data Used in Model Calibration**

In addition to being used to generate an initial head distribution, the water-level measurements made in 35 wells within the model domain during late 2000 were also used in steady-state model calibration. (Note that Table TFIELD-5 includes data from two wells – WIPP-27 and WIPP-29 – that were used to define model boundary conditions but are outside the area of calibration).

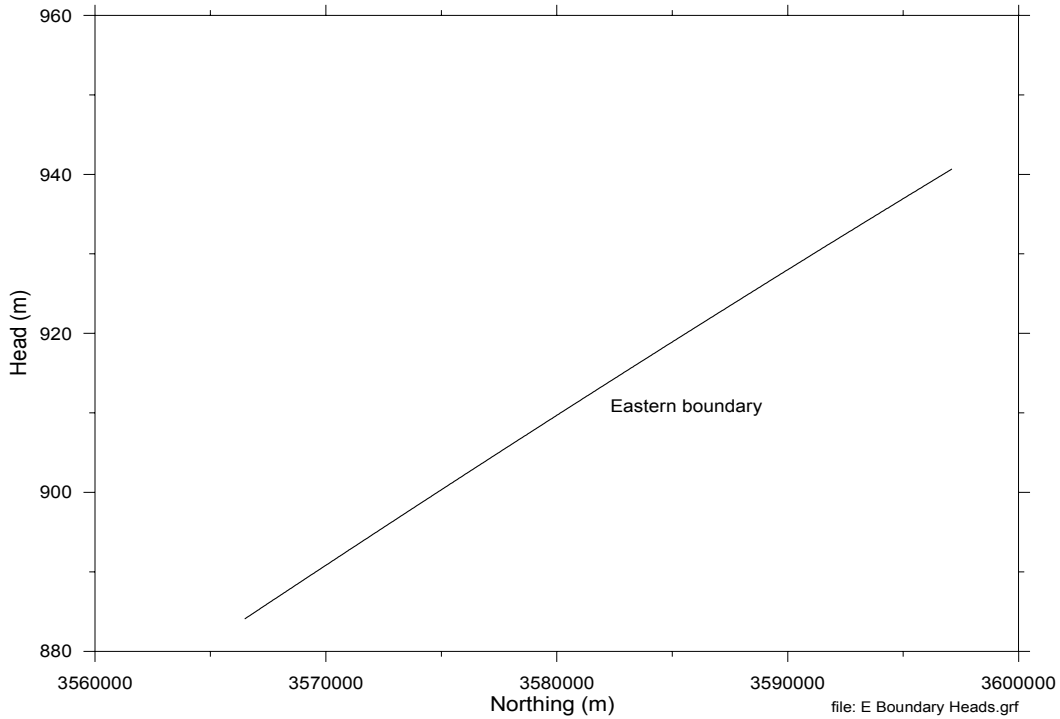
The transient observation data used for the transient calibrations were taken from a number of different sources listed in Beauheim (2003a). Responses to seven different hydraulic tests were employed in the transient portion of the calibration (Table TFIELD-8). Hydraulic responses for each of the seven tests were monitored in three to ten different observation wells depending on the hydraulic test.

1



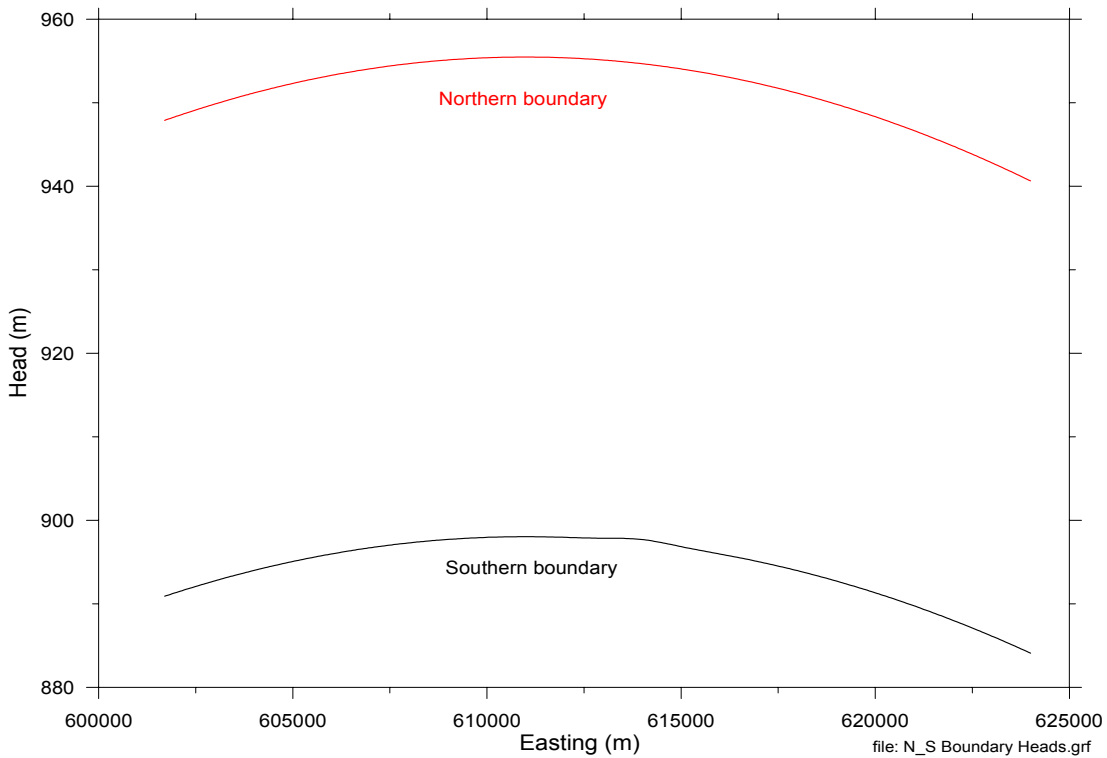
2

3 **Figure TFIELD-20. Map of Initial Heads Created Through Kriging and Used to Assign**
4 **Fixed-Head Boundary Conditions**



1
2
3

Figure TFIELD-21. Values of Fixed Heads Along the Eastern Boundary of the Model Domain



4
5
6

Figure TFIELD-22. Values of Fixed Heads Along the Northern and Southern Boundaries of the Model Domain. Note that not all locations along the boundaries are active cells.

1
2

**Table TFIELD-8. Transient Hydraulic Test and Observation Wells
for the Drawdown Data**

Stress Point	Observation Well	Observation Start	Observation End	Observation Type
H-3b2	DOE-1	10/15/1985	3/18/1986	Drawdown
	H-1	10/15/1985	4/14/1986	Drawdown
	H-2b2	10/15/1985	4/2/1986	Drawdown
	H-11b1	10/15/1985	4/21/1986	Drawdown
WIPP-13	DOE-2	1/12/1987	5/15/1987	Drawdown
	H-2b2	1/12/1987	5/15/1987	Drawdown
	H-6b	1/12/1987	5/15/1987	Drawdown
	P-14	1/12/1987	5/15/1987	Drawdown
	WIPP-12	1/12/1987	5/15/1987	Drawdown
	WIPP-18	1/12/1987	5/15/1987	Drawdown
	WIPP-19	1/12/1987	5/15/1987	Drawdown
	WIPP-25	1/12/1987	4/2/1987	Drawdown
	WIPP-30	1/12/1987	5/15/1987	Drawdown
P-14	D-268	2/14/1989	3/7/1989	Drawdown
	H-6b	2/14/1989	3/10/1989	Drawdown
	H-18	2/14/1989	3/10/1989	Drawdown
	WIPP-25	2/14/1989	3/7/1989	Drawdown
	WIPP-26	2/14/1989	3/7/1989	Drawdown
H-11b1	H-4b	2/7/1996	12/11/1996	Drawdown
	H-12	2/6/1996	12/10/1996	Drawdown
	H-17	2/6/1996	12/10/1996	Drawdown
	P-17	2/7/1996	12/10/1996	Drawdown
H-19b0	DOE-1	12/15/1995	12/10/1996	Drawdown
	ERDA-9	12/15/1995	12/10/1996	Drawdown
	H-1	12/15/1995	12/10/1996	Drawdown
	H-14	2/7/1995	12/10/1996	Drawdown
	H-15	12/12/1995	12/10/1996	Drawdown
	H-2b2	2/7/1996	12/10/1996	Drawdown
	H-3b2	12/15/1995	12/10/1996	Drawdown
	WIPP-21	1/18/1996	12/9/1996	Drawdown
	WQSP-4	1/1/1996	12/10/1996	Drawdown
WQSP-5	1/18/1995	12/10/1996	Drawdown	
WQSP-1	H-18	1/25/1996	2/20/1996	Drawdown
	WIPP-13	1/25/1996	2/20/1996	Drawdown
	WQSP-3	1/15/1996	2/20/1996	Zero Response
WQSP-2	DOE-2	2/20/1996	3/28/1996	Drawdown
	H-18	2/20/1996	3/28/1996	Drawdown
	WIPP-13	2/20/1996	3/28/1996	Drawdown
	WQSP-1	2/20/1996	3/24/1996	Drawdown
	WQSP-3	2/20/1996	3/24/1996	Zero Response

3

4 A major change in the calibration data set from the CCA calculations is the exclusion of the
5 hydraulic responses to the excavation of the exploratory (now salt) and ventilation (now waste)
6 shafts in the current calibration. The responses to the shaft excavations were excluded because:

- 1 1. Only two wells (H-1 and H-3) responded directly to the shaft excavations and the areas
2 between the shafts and these wells are stressed by other hydraulic tests that are included
3 in the calibration data set (H-3b2, WIPP-13, and H-19b0).

- 4 2. It was difficult to model both the flux and pressure changes accurately during the
5 excavation of the shafts with MODFLOW-2000. This difficulty is due to both the finite-
6 difference discretization of MODFLOW-2000 that requires each shaft to be modeled as a
7 complete model cell and some limitations of the data set.

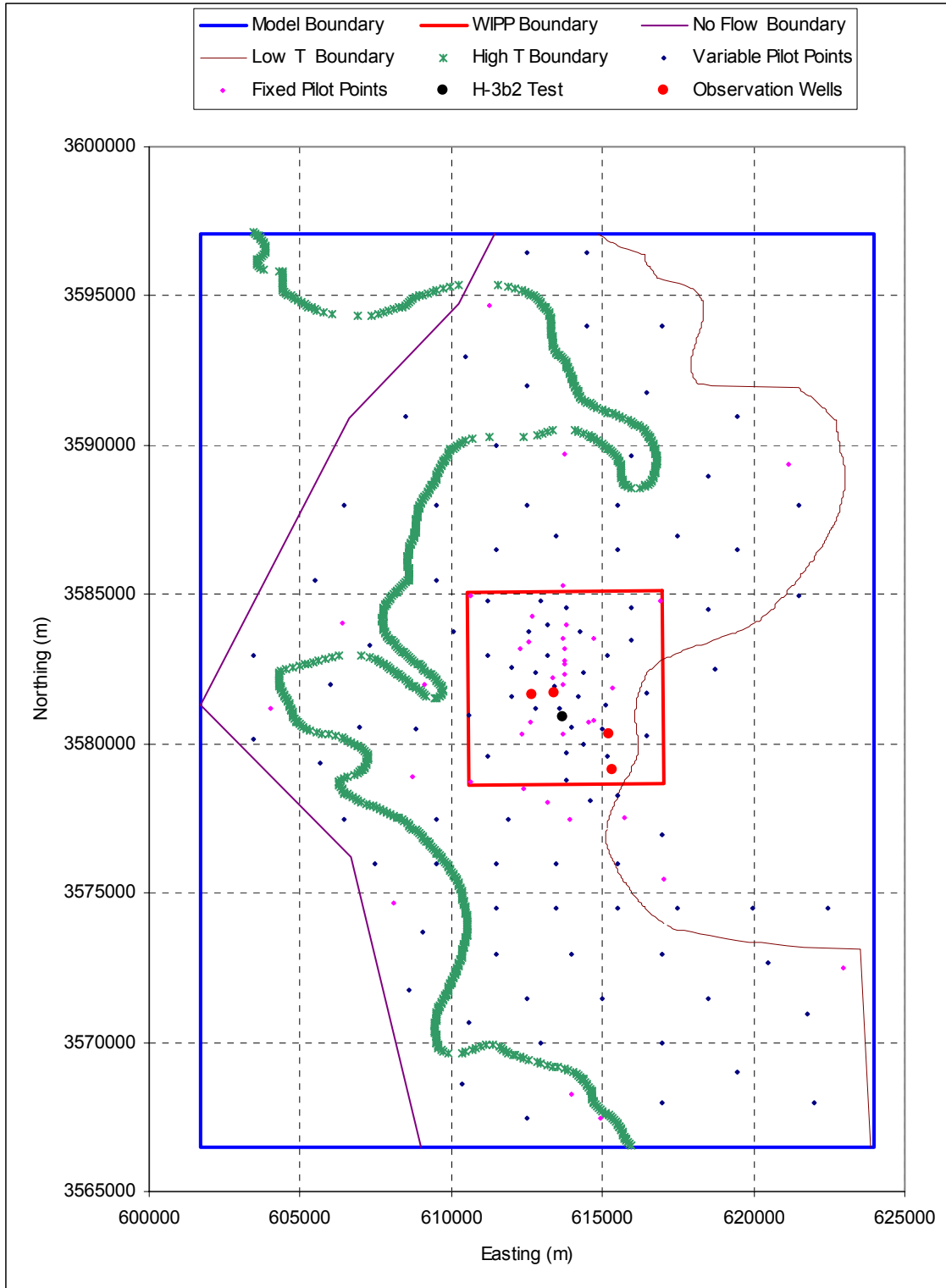
- 8 3. The long-term effects of the shafts on site-wide water levels were important for the CCA
9 modeling because that modeling sought to replicate heads over time. In the current CRA-
10 2004 calibration effort, shaft effects are not important because drawdowns resulting from
11 specific hydraulic tests are used as the calibration targets and shaft effects can be
12 considered as second-order compared to the effects of the hydraulic tests that are
13 simulated.

14 A small amount of processing of the observed data was necessary prior to using it in the
15 calibration process. This processing included selecting the data values that would be used in the
16 calibration procedure from the often voluminous measurements of head. These data were chosen
17 to provide an adequate description of the transient observations at each observation well across
18 the response time without making the modeling too computationally burdensome in terms of the
19 temporal discretization necessary to model responses to these observations. Scientific judgment
20 was used in selecting these data points. This selection process resulted in a total of 1,332
21 observations for use in the transient calibration.

22 Additionally, the modeling of the pressure data is done here in terms of drawdown. Therefore,
23 the value of drawdown at the start of any transient test must be zero. A separate perl script was
24 written to normalize each set of observed heads to a zero value reference at the start of the test
25 with the exception of the H-3 test that is only preceded by the steady-state simulation. The
26 calculations are such that the resulting drawdown values are positive.

27 In addition to normalizing the measured head data, some of the tests produced negative
28 drawdown values when normalized. These negative results are due to some of the observations
29 having heads greater than the reference value. This occurs due to some hydraulic tests that were
30 conducted at earlier times in the Culebra but were not included in the numerical model. If the
31 drawdowns from one of these previous tests are still recovering to zero at the start of a
32 simulation, they can cause negative drawdowns in the simulation as the recovery continues.
33 Most of these effects were addressed through trend removal in initial data processing (Beauheim
34 2003a) but some residual effects remain.

35 The resultant transient calibration points are shown in Figures TFIELD-23 through TFIELD-36.
36 These sets of figures show the location of each hydraulic test and the locations of the observation
37 wells for that test within the model domain and the time series of drawdown values for each



1
2 **Figure TFIELD-23. Locations of the H-3b2 Hydraulic Test Well and Observation Wells**

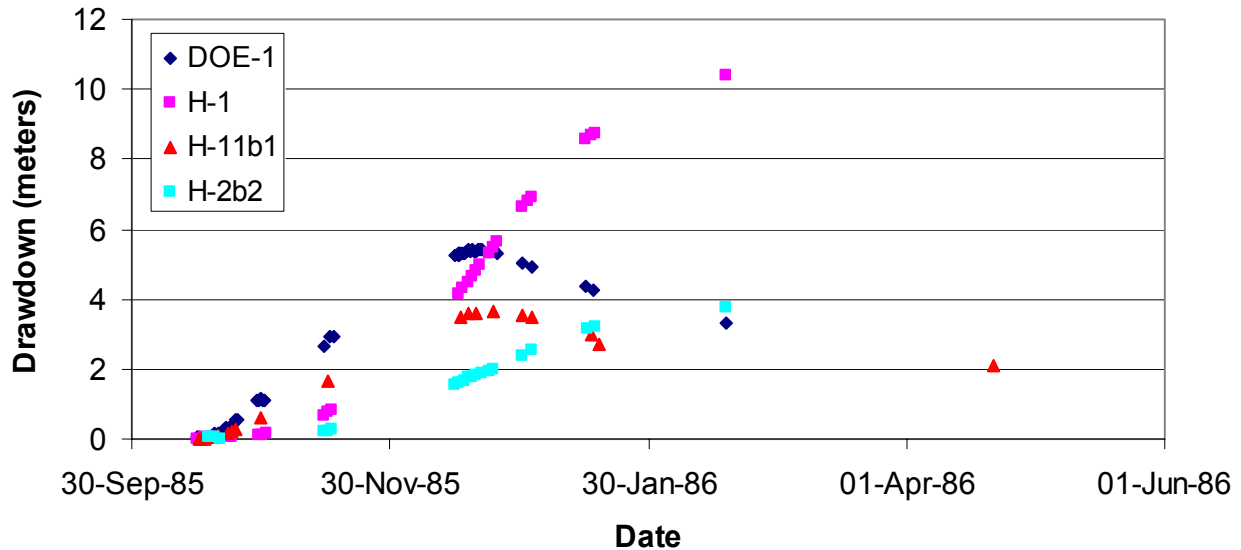


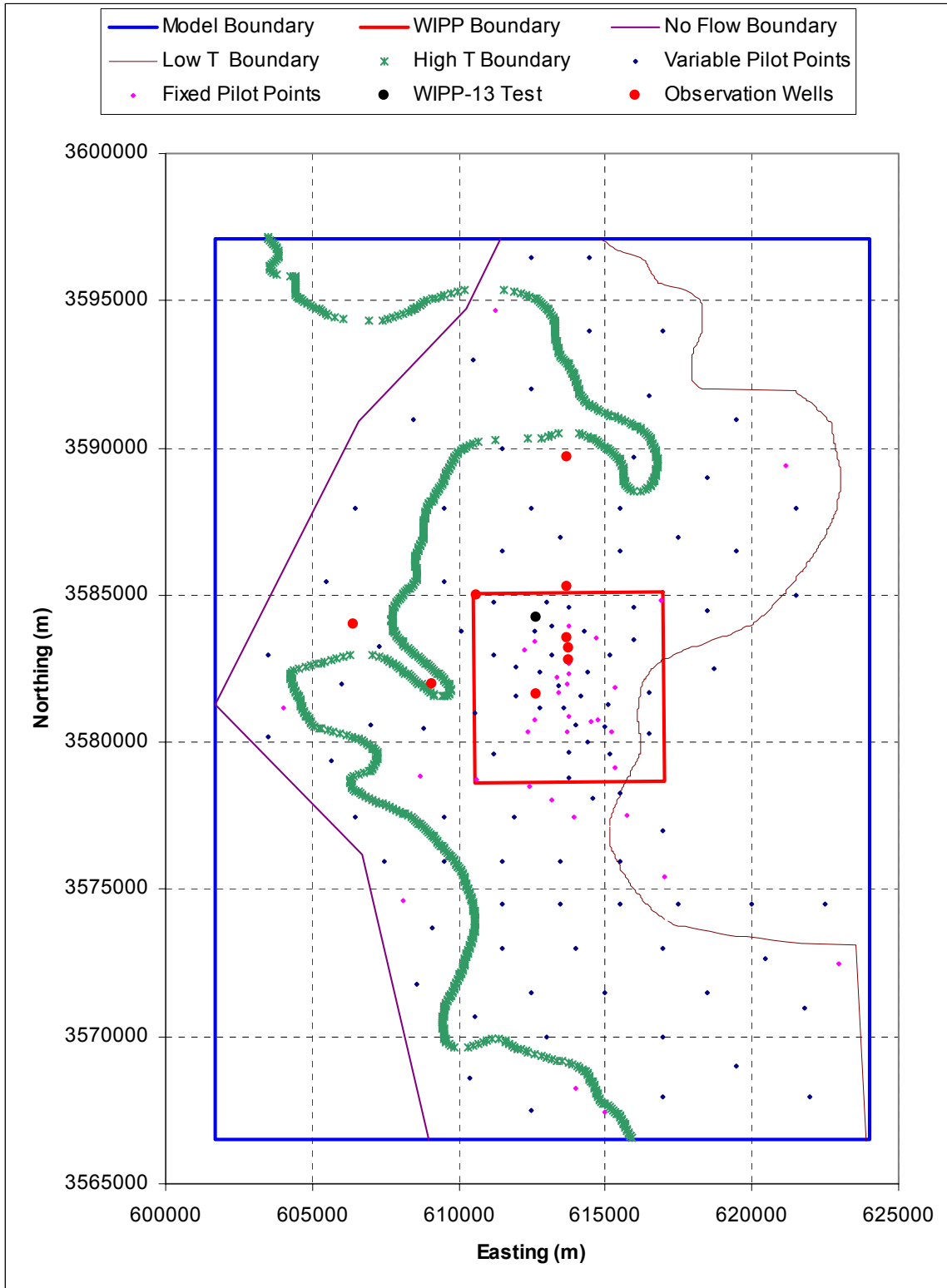
Figure TFIELD-24. Observed Drawdowns for the H-3b2 Hydraulic Test

observation well. The values of drawdown are in meters where a positive drawdown indicates a decrease in the pressure within the well relative to the pressure before the start of the pumping (negative drawdown values indicate rises in the water level). For the WQSP-1 and WQSP-2 tests, well WQSP-3 showed no response. These results are used in the calibration process by setting the observed drawdown values to zero for WQSP-3. The maps in Figures TFIELD-23 through TFIELD-35 also show the locations of the pilot points used in the calibration (these are discussed later).

TFIELD-6.5 Spatial Discretization

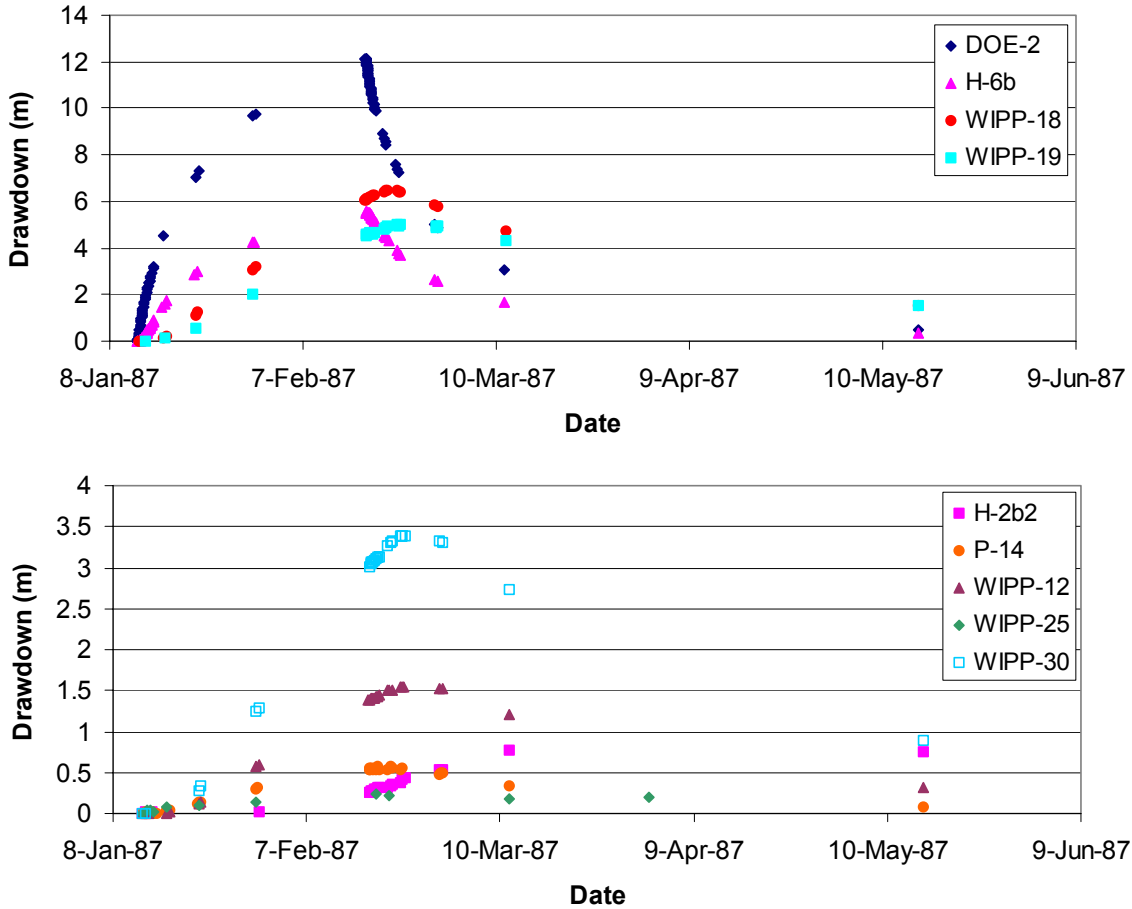
The flow model was discretized into 68,768 regular, orthogonal cells each of which is 100 m (328 ft) \times 100 m (328 ft). A constant Culebra thickness of 7.75 m (25.4 ft) was used (CCA Appendix TFIELD.4.1.1, Culebra:Thick). The 100-m (328-ft) grid discretization was selected to make the finite-difference grid cell sizes considerably finer, on average, than those used in the CCA calculations, but still computationally tractable. In the CCA calculations, a telescoping finite-difference grid was used with the smallest cell being 100 m (328 ft) \times 100 m (328 ft) near the center of the domain. The largest cells in the CCA flow model grid were 800 m (2,625 ft) \times 800 m (2,625 ft) near the edges of the domain (Lavenue, 1996).

The cells in the model domain were assigned elevations based on the digitized version of Figure TFIELD-1. Of the 68,768 cells (224 east-west by 307 north-south), 14,999 (21.8 percent) lie to the west of the no-flow boundary, so the total number of active cells in the model is 53,769. This number is nearly a factor of five larger than the 10,800 (108 \times 100) cells used in the CCA calculations.



1
2
3

Figure TFIELD-25. Locations of the WIPP-13 Hydraulic Test Well and Observation Wells

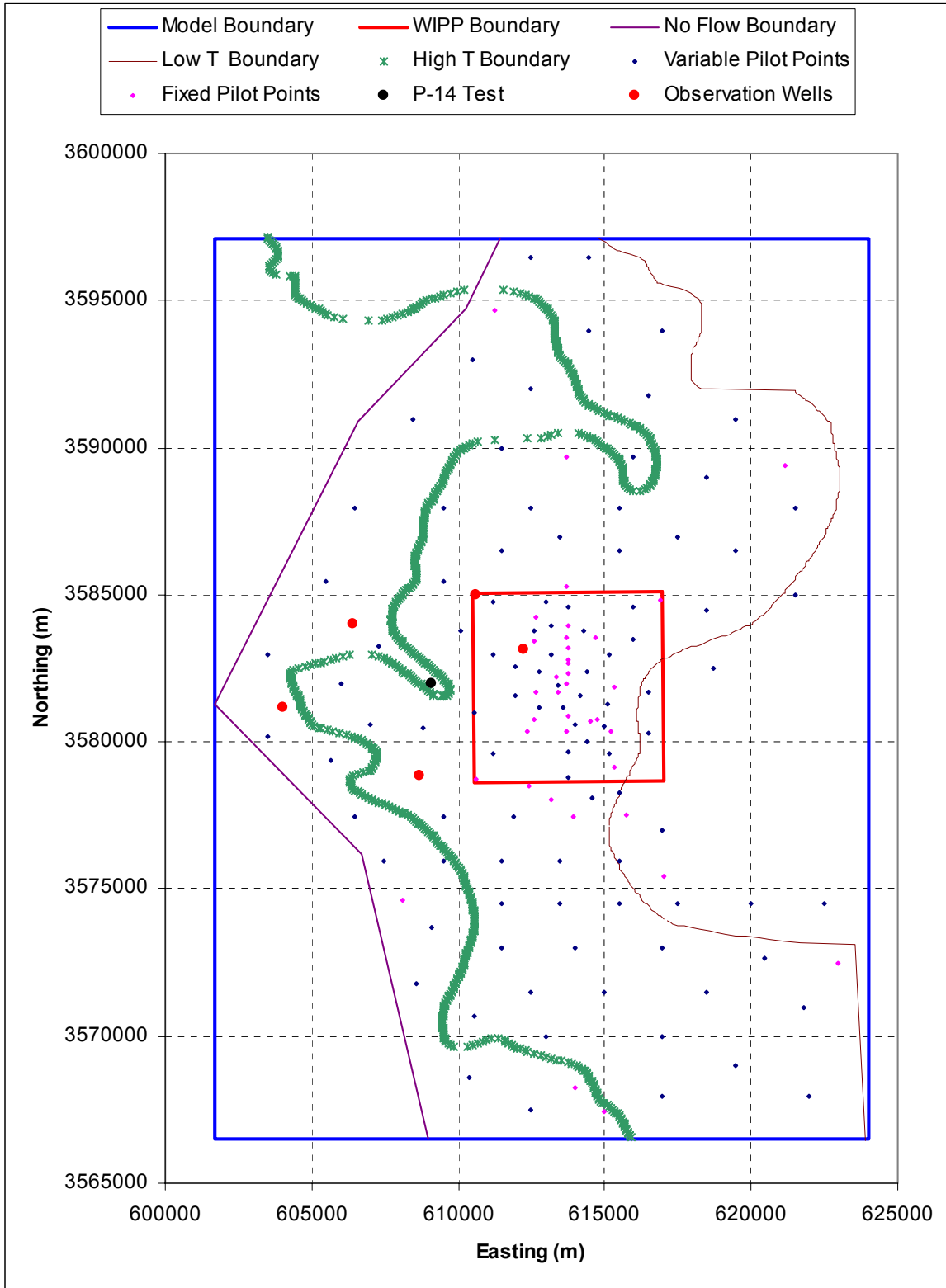


1
 2 **Figure TFIELD-26. Observed Drawdowns for the WIPP-13 Hydraulic Test. Note the**
 3 **change in the scale of the Y-axis from the upper to the lower image.**

4 ***TFIELD-6.6 Temporal Discretization***

5 The time period of nearly 11 years and 2 months covered by the transient modeling began
 6 October 15, 1985 and ended December 11, 1996. Additionally, a single steady-state calculation
 7 was run prior to the transient modeling. The length of this steady-state time period and the date
 8 at which it occurs were arbitrarily set to one day (86,400 s) occurring from October 14, 1985, to
 9 October 15, 1985. These steady-state heads were measured in the year 2000 and were only set to
 10 these October dates to provide a steady-state solution prior to the start of any transient hydraulic
 11 events. The responses to the transient events were defined by the amount of drawdown relative
 12 to the initial steady-state solution. The discretization of this time interval was dictated by the
 13 pumping history of the different wells used in the hydraulic testing and consideration of the
 14 additional computational burden required for increasingly fine time discretization.

15 The groundwater flow model, MODFLOW-2000, allows for the discretization of time into both
 16 “stress periods” and “time steps.” A stress period is a length of time over which the boundary
 17 conditions and internal stresses on the system are constant. Even though these stresses are
 18 constant, this does not mean that the flow system is necessarily at steady state during the stress



1

2

Figure TFIELD-27. Locations of the P-14 Hydraulic Test Well and Observation Wells

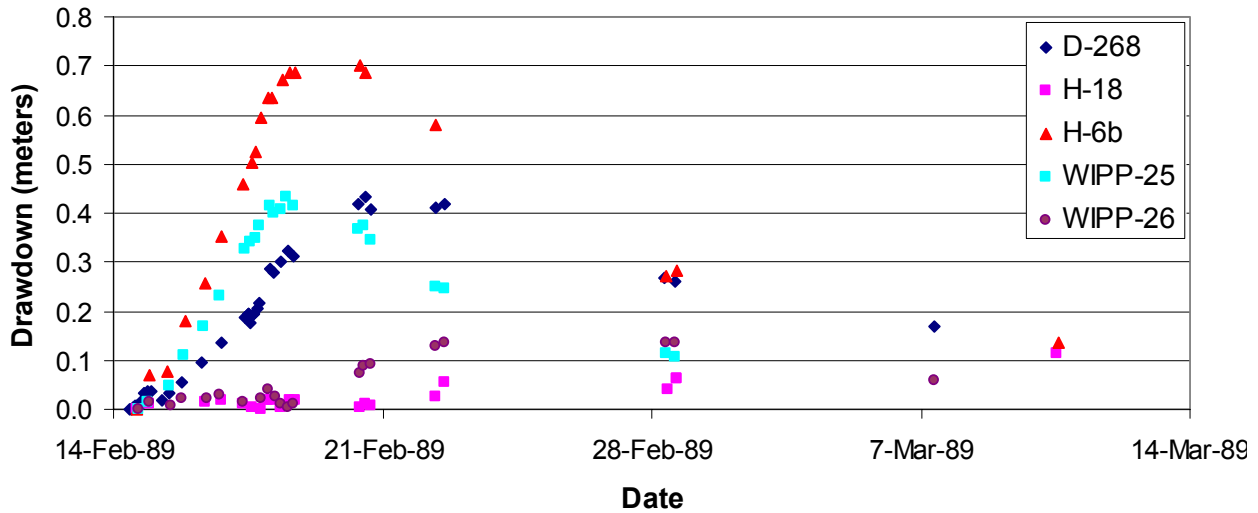
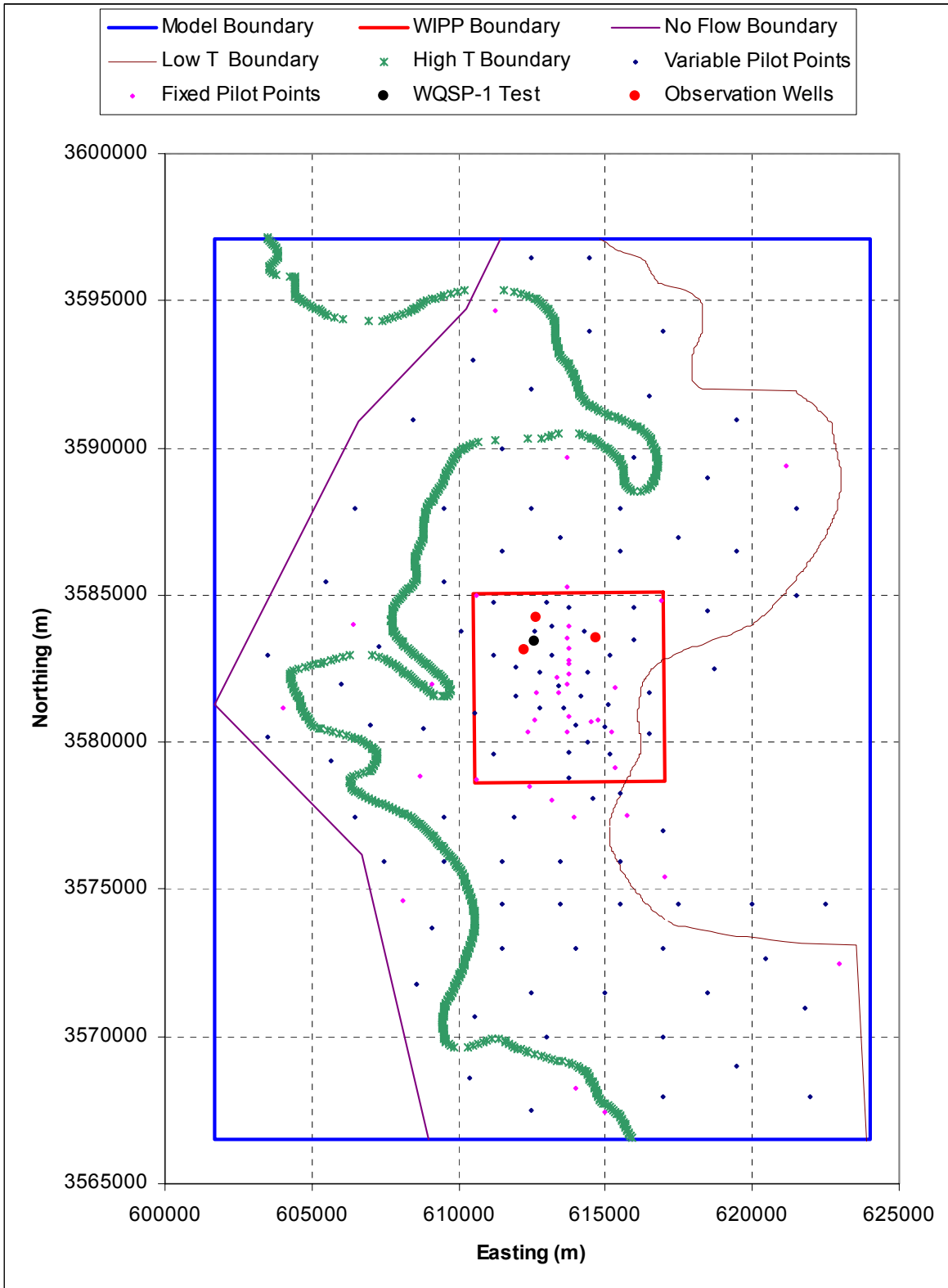


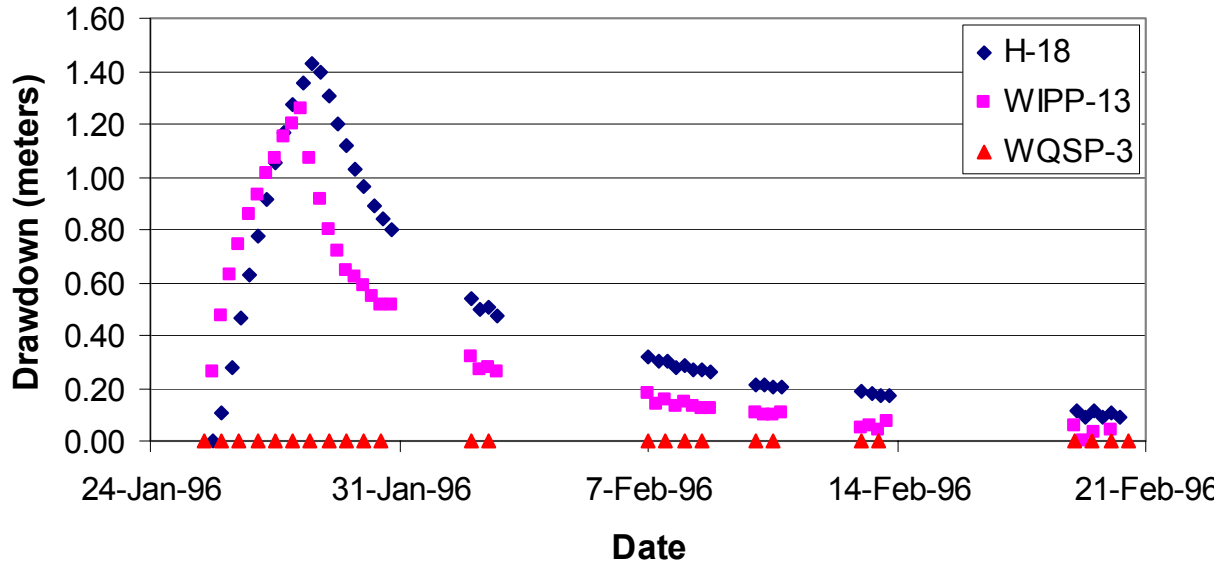
Figure TFIELD-28. Observed Drawdowns for the P-14 Hydraulic Test

period. A time step is a subdivision of a stress period. System information such as the head or drawdown values is only calculated at the specified time steps. Each stress period must contain at least one time step. MODFLOW-2000 allows for the specification of the stress period length, the number of time steps in the stress period, and a time step multiplier. The time step multiplier increases the time between successive time steps geometrically. This geometric progression provides a nearly ideal time discretization for the start of a pumping or recovery period. To save on computational costs associated with calculating head/drawdown at each time step and with writing out the heads/drawdowns, the number of time steps in the model was kept to the minimum number possible that still adequately simulated the hydraulic tests. The time discretization in MODFLOW-2000 resulted in modeled heads calculated at times that sometimes differed from the observation times. For this situation, the PEST utility, mod2obs, was used to interpolate the head, or drawdown, values in time from the simulation times to the observation times.

A summary of the time discretization is given in Table TFIELD-9. There are five separate MODFLOW-2000 simulations for each complete forward simulation of the transient events. Each separate call to MODFLOW-2000 has its own set of input and output files. In Table TFIELD-9, each call to MODFLOW-2000 is separated by a horizontal black line. The first call is the steady-state simulation. The second, third, and fourth calls to MODFLOW-2000 (H-3, WIPP-13, and P-14) are all similar in that a single well was pumped. For the H-3 and WIPP-13 calls, there were a total of three stress periods. In the first stress period, the well was pumping at a constant rate; in the second stress period, the pumped well was inactive and heads were recovering after the cessation of pumping; and the final stress period was simply a long time of no pumping activity used to advance the simulation time to be consistent with the calendar time. The first two stress periods were discretized using eight time steps and the final stress period with no pumping activity was discretized using the minimum possible number of time steps—one.



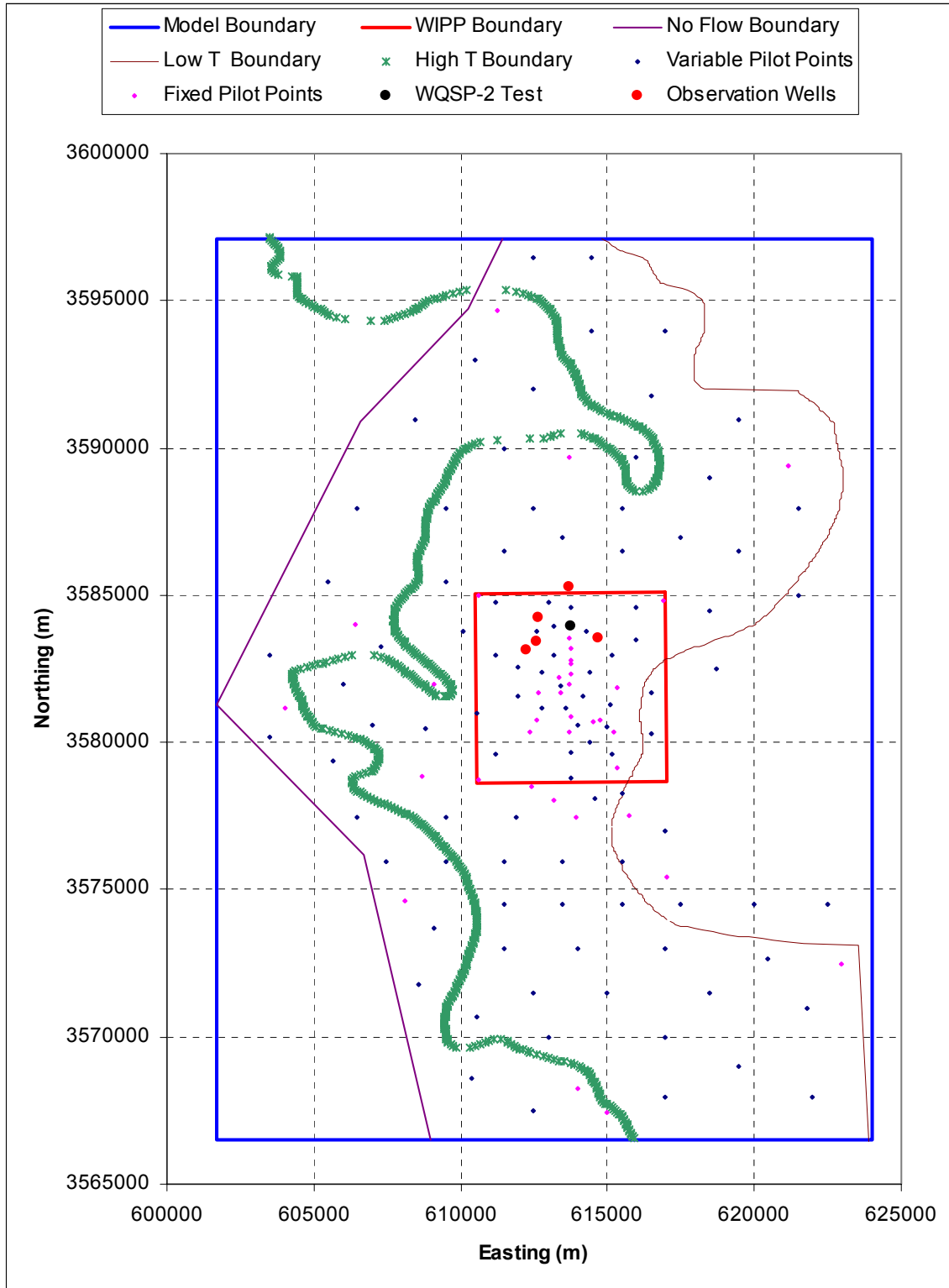
1
2 **Figure TFIELD-29. Locations of the WQSP-1 Hydraulic Test Well and Observation Wells**
3



1
2 **Figure TFIELD-30. Observed Drawdowns for the WQSP-1 Hydraulic Test**

3 The final MODFLOW-2000 call, the H-19 call, was considerably more complicated than the
4 earlier calls to MODFLOW-2000 and simulated the hydraulic conditions during the H-11, H-19,
5 WQSP-1, and WQSP-2 hydraulic tests. This final call contained 17 stress periods with as many
6 as three different wells pumping during any single stress period. The pumping rates of the
7 different wells in this call to MODFLOW-2000 and the stress periods are shown as a function of
8 time in Figure TFIELD-37. The first six stress periods in this call simulated pumping in the
9 H-19 and H-11 wells without any observations (Table TFIELD-9). These pumping periods were
10 added to the model solely to account for the effects of these tests in observations of later
11 hydraulic tests and, therefore, these tests could be modeled with a single time step. The pumping
12 rates shown in Figure TFIELD-37 are given as negative values to indicate the removal of water
13 from the Culebra following the convention used in MODFLOW-2000.

14 The MODFLOW-2000 simulations could be done using a single call to MODFLOW-2000, but
15 five separate calls were used here. Each of the five calls created separate binary output files of
16 drawdown and head that were much smaller and easier to manage than a single output file would
17 have been. Additionally, the simulated drawdowns at the start of each transient test must be zero
18 (no drawdown prior to pumping). Because MODFLOW-2000 uses the resulting drawdowns and
19 heads from the previous stress period as input to the next stress period, a single simulation would
20 not necessarily start each transient test with zero drawdowns. Calling MODFLOW-2000 five
21 times allowed the initial drawdowns to be reset to zero each time using shell scripts. The heads
22 simulated at the end of the final time step in each MODFLOW-2000 call were used as the initial
23 heads for the next call. The results of all five calls were combined to produce the 1332 model
24 predictions prior to comparing them to the 1332 selected observation data, thus ensuring that all
25 steady-state and transient data were used simultaneously in the inverse calibration procedure.



1
2 **Figure TFIELD-31. Locations of the WQSP-2 Hydraulic Test Well and Observation Wells**

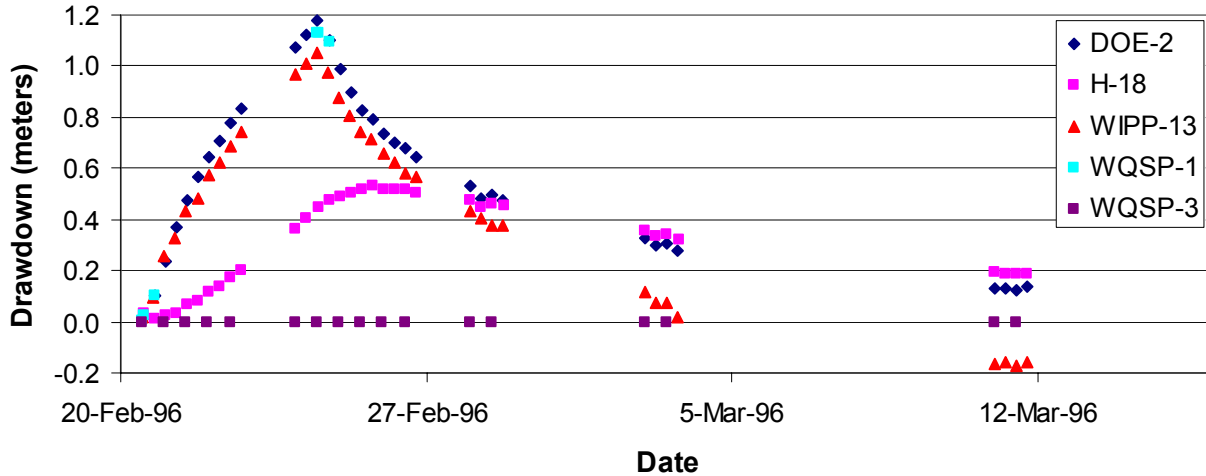
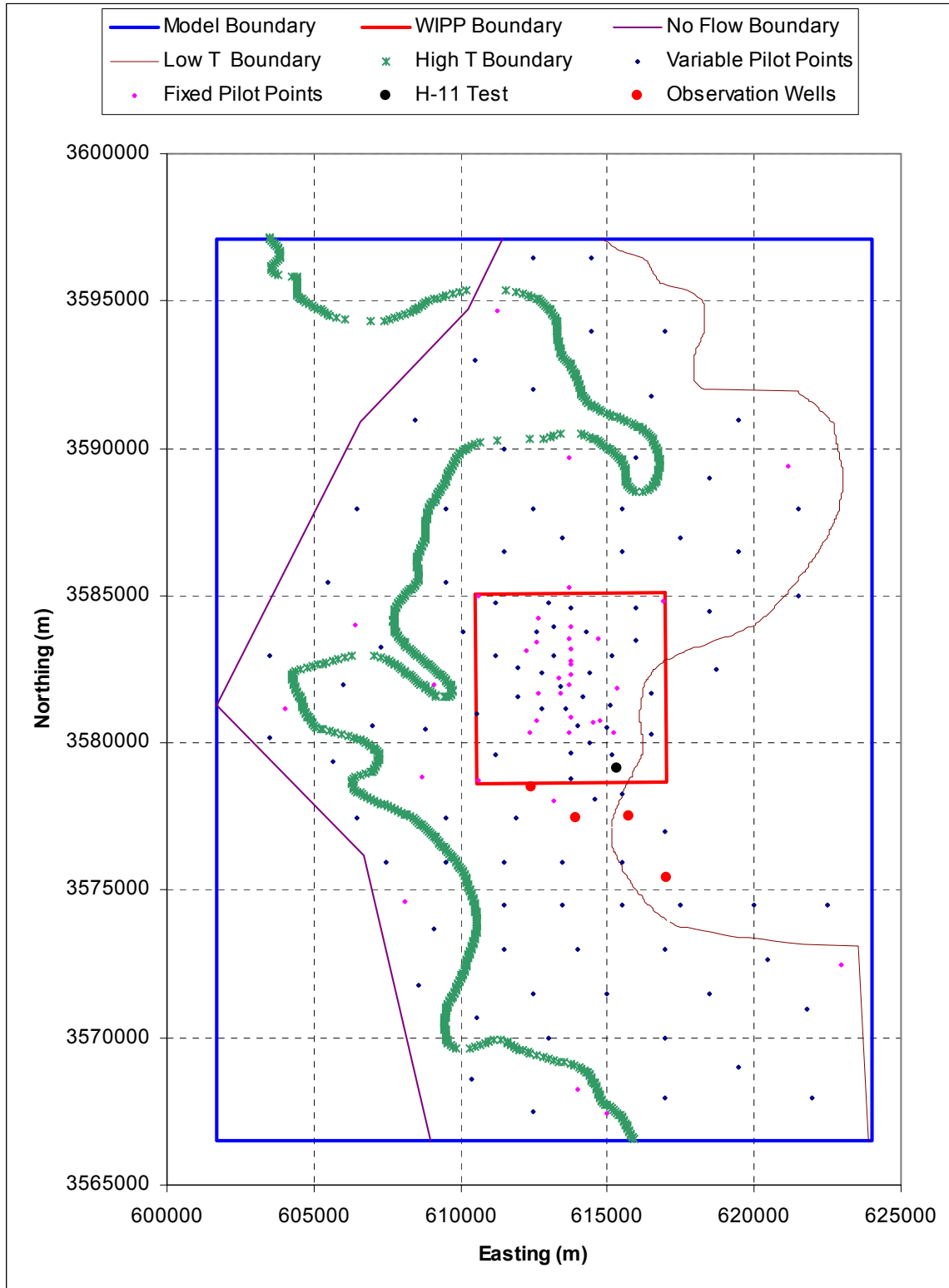


Figure TFIELD-32. Observed Drawdowns from the WQSP-2 Hydraulic Test

TFIELD-6.7 Weighting of Observation Data

The observed data for each response to each transient hydraulic test are weighted to take into account the differences in the responses across the different tests. The weights are calculated as the inverse of the maximum observed drawdown for each hydraulic test. This weighting scheme applies relatively less weight to tests with large drawdowns and relatively more weight to tests with smaller responses. This weighting scheme was used so that the overall calibration was not dominated by trying to reduce the very large residuals that may occur at a few of the observation locations with very large drawdowns. Under this weighting scheme, two tests that are both fit by the model to within 50 percent of the observed drawdown values would be given equal consideration in the calculation of the overall objective function even though one test may have an observed maximum drawdown of 10 m (33 ft) and the other a maximum observed drawdown of 0.10 m (0.33 ft).

The weights assigned in this manner ranged from 0.052 to 20.19. The observed absence of a hydraulic response at WQSP-3 to pumping at WQSP-1 and WQSP-2 was also included in the calibration process by inserting measurements of zero drawdown that were given an arbitrarily high weight of 20. Through trial and error using the root mean squared error criterion of how well the modeled steady-state heads fit the observed steady-state heads, a weight of 2.273 was assigned to the 35 steady-state observations. This weight is near that of the average of all the weights assigned to the transient events and was found to be adequate to provide acceptable steady-state matches. It is noted that the steady-state data provide measurements of head while all of the transient events provide measurements of drawdown. However, the weights were applied to the residuals between the observed and modeled aquifer responses and because both heads and drawdowns are measured in meters, there was no need to adjust the weights to account for different measurement units.



1
2

Figure TFIELD-33. Locations of the H-11 Hydraulic Test Well and Observation Wells